VPP Driven Parametric Design of AC75 Hydrofoils

Rafael Tannenberg
University of Southampton, UK, rafael.tannenberg@soton.ac.uk.

Stephen R. Turnock
University of Southampton, UK.

Karsten Hochkirch
DNV Ship Performance Center, Germany.

Stephen W. Boyd
University of Southampton, UK.

Abstract. Hydrofoils are a vital part of modern racing yachts such as the AC75, which was sailed in the 36th America's Cup and should hence be optimised thoroughly. The literature shows that hydrofoil design and optimisation usually focuses on the lift and drag characteristics in isolation of the yacht 'system'. Although these characteristics relate to hydrofoil performance, they do not directly translate to the performance of the yacht on the race course. In this paper we perform a parametric study of the main design variables of the hydrofoil that is based on a model of the entire yacht in the Velocity Prediction Program (VPP) FS-Equilibrium. The hydrofoil forces are modelled using an advanced lifting line method and empirical formulations for a bulb. This accurately captures the foil design influence on the boat´s performance. The VPP is coupled to a parametric model of the foil based on NURBS surfaces (Non-uniform rational B-Splines) which was used to systematically generate 72 different designs. The candidates were tested in three wind speeds for up and downwind performance. The best performing design has maximum span and anhedral angle, and minimum chord with some of the weight stored in a bulb. The study shows that the assessment of hydrofoils where the performance is measured in boat speed is an extremely valuable tool.

Keywords: Velocity Prediction; Hydrofoil; Parametric Study; Optimisation; AC75.

NOMENCLATURE

A_i	Area of segment i [m^2]
A_F	Foretriangle area [m^2]
A_J	Jib area [m^2]
A_M	Mainsail area [m^2]
A_N	Nominal area [m^2]
A_R	Aspect ratio
C_D	Drag coefficient
C_{Di}	Induced drag coefficient
C_{Dpj}	Jib profile drag coefficient
C_{Dpm}	Mainsail profile drag coefficient
C_H	Heeling force coefficient
C_L	Lift coefficient
C_{Lj}	Jib lift coefficient
C_{Lm}	Mainsail lift coefficient

C_R Driving force coefficient

c Chord length [m]

d_z Sink (ride height) [m]

E_{HM} Mast height above shear [m]

F_A Average shear height [m]

$\boldsymbol{F_i}$ Force at control point i [N]

f_i Function i

f_x Force in x-direction [N]

f_y Force in y-direction [N]

f_z Force in z-direction [N]

h Submersion [m]

l_i Lagrangian multiplier i

$\boldsymbol{l_i}$ Length of segment i [m]

$N_{\mathrm{i,p}}(u)$ Nonrational B-spline basis function in u-direction

$N_{\mathrm{j,q}}(v)$ Nonrational B-spline basis function v-direction

m_x Moment around x-axis [Nm]

m_y Moment around y-axis [Nm]

m_z Moment around z-axis [Nm]

p, q Degrees of NURBS surfaces in u- and v-direction

$P_{\mathrm{i,j}}$ Control points of NURBS-Surfaces

R_F Frictional resistance [N]

R_T Total resistance [N]

S NURBS surface

s Span [m]

t Thickness [m]

u, v Directions of NURBS surfaces

$\boldsymbol{V_i}$ Local velocity at control point i [m s^{-1}]

V_{MG} Velocity made good [kts]

V_S Boat speed [kts]

V_{TW} True wind speed [kts]

$\boldsymbol{V}_\infty$ Free-stream velocity [m s^{-1}]

$\boldsymbol{v_{\mathrm{ji}}}$ Influence of horseshoe vortex j on control point i [m^{-1}]

$w_{\mathrm{i,j}}$ Weights of control points of NURBS surfaces

$(1+k)$ Form factor

β_a Apparent wind angle [°]

β_t True wind angle [°]

Γ_j Strength of horseshoe vortex j [m^2 s^{-1}]

δ_e Elevator rake [°]

δ_f Flap angle [°]

δ_r Rudder angle [°]

θ Pitch angle [°]

λ Leeway angle [°]

$\boldsymbol{\xi}$ Free variable vector

ρ Density [kg m^{-3}]

τ flat parameter

φ Heel angle [°]

ETNZ   Emirates Team New Zealand

IMS   International Measurement System

NURBS   Non-uniform rational B-Splines

VPP   Velocity prediction program

1. INTRODUCTION

The 36th America´s Cup saw the introduction of the first fully foiling monohull yacht class, the AC75, in Auckland in 2020. The yachts were sailed with great success and reached speeds above 53 kts that were not seen in the previous America's Cups. The AC75 was also appointed as the class for the 37th America´s Cup which will be held in Barcelona in 2024. The design class allows development in certain areas within the rules originally set out by the Royal New Zealand Yacht Squadron and the Circolo Della Vela Sicilia (2020). This includes the design of the hydrofoils which has proven to be extremely important as it has a huge influence on the performance of the yachts. Figure 1 shows the AC75 with its two main hydrofoils. The windward foil of the AC75 is canted out of the water to provide righting moment while the leeward foil is canted into the water to generate hydrodynamic lift. The foils are equipped with flaps that can be used to control the amount of hydrodynamic force generated. The cant angle of the leeward foil can be changed to adjust the ratio of generated side force to vertical lift as well as the amount of generated righting moment. The hydrofoil can be divided into two parts: the foil arm and the foil wing, both shown in Figure 1. The design of the foil arm is mainly fixed by the rule while the foil wing geometry is open to development within the `Foil box´ shown in Figure 2. The wing must be symmetric around the `Foil wing symmetry plane´ and must be placed within 10 and 12 m forward of the transom. In addition, the wing, the flaps and the internal control systems must weigh 921 kg to ensure the yacht has a reasonable amount of righting moment. To meet this weight requirement, while enabling a wing with low volume and low associated wetted surface area, the wings are made from a combination of steel and lead. The design space also allows a bulb to incorporate some of the weight. Emirates Team New Zealand (ETNZ) and American Magic chose to use bulbs and wings with smaller chord, while Luna Rossa and INEOS Team UK chose wings with larger chord and no bulb. Further differences included different taper ratios and anhedral angles. ETNZ's foil had no anhedral angle (T-Foil), while the other teams opted for Y-Foils as seen in Figure 1.

Figure 1. AC75 Luna Rossa based on Gattini (2020).

This work investigates 72 different hydrofoil designs with varying extension lengths (which translate to different anhedral angles), semi spans, root chords, taper ratios and wing rakes. The weight of every candidate is computed and a bulb is automatically sized to meet the weight requirement. The study includes design candidates that approximately represent the foils of the four teams in the last America´s Cup. The designs are evaluated in terms of their performance in up- and downwind conditions in the three true wind speeds (V_{TW}) 8, 11 and 14 kts using the VPP FS-Equilibrium. Although the AC75 rule has slightly changed for the next edition (Royal New Zealand Yacht

Squadron and Royal Yacht Squadron, 2023), the performance predictions in this study are based on the original rule to enable meaningful comparison with publicly available performance data from the last America´s Cup.
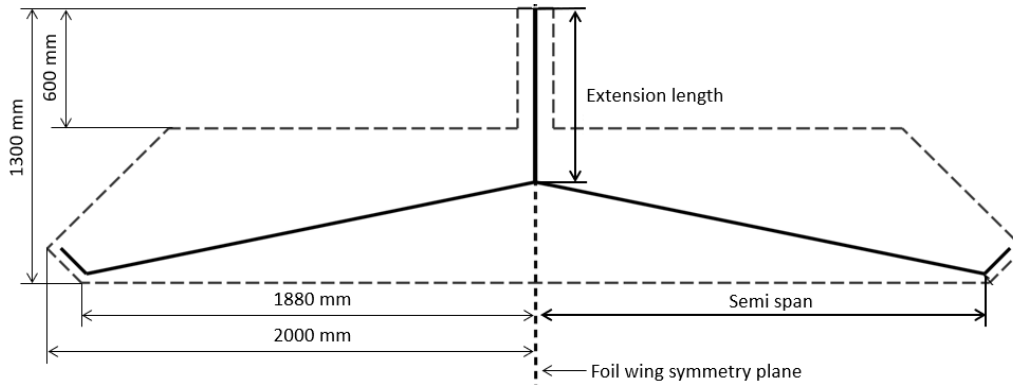

Figure 2. Foil Box.

2. VELOCITY PREDICTION MODEL

FS-Equilibrium is a common workbench for the analysis of stationary and dynamic states of sailing yachts. The different forces acting on a yacht are modelled in so called 'force modules' for given conditions. A state for which the forces from the modules equate to zero in all degrees of freedom is called a valid steady sailing state. The program determines the steady sailing state by means of a Newton-Raphson method. The method alters the state variables of the yacht until force equilibrium is found. A Hooke-Jeeves algorithm can be used on top to maximise the performance of the yacht by optimising the trim variables. For example, common trim variables are the *flat*-parameter for the depowering of sails or the position of the crew. FS-Equilibrium has been successfully used for hydrofoiling boats in the past such as the C-Class Catamaran Groupama (Paulin et al, 2015), the International Moth (Eggert, 2018), the AC50 (Hansen et al, 2019) and the QFX Lake Racer (Melis et al, 2022). For more information on the VPP see Hochkirch (2018).

2.1 SOLVER SET-UP

The stationary mode of FS-Equilibrium was used to compute the steady sailing states of the AC75. It is limited to the states where the boat is fully foiling. This increases the robustness of the solver while it does not affect the evaluation of a foil´s performance because the only foil designs considered are those that can fully support the yacht in all evaluated conditions. However, the AC75 is sailed very differently compared to normal displacement yachts, which must be reflected in the set-up of the solver. In contrast to a traditional sailing yacht the trimming of the boat is much more dynamic and a non-optimum trim might lead to a capsize instead of a valid sailing state which is just slightly slower. Table 1 shows the state variables (blue) and trim variables (grey) that the Newton-Raphson uses to balance the individual forces and moments for a conventional sailing yacht and the AC75. As for conventional yachts, the boat speed V_S, the leeway angle λ and the rudder angle δ_r are employed to balance f_x, f_y and m_z, respectively. f_z however, must be balanced by a trim variable as the AC75 foils are not passively controlling the ride height. Hence, the state variable `ride height´ (or sink) $d_z$ has little influence on the heave forces as long as the yacht is fully foiling. The trim variable `flap angle´ δ_f must be employed instead. Furthermore, the moments around the x-axis (m_x) must be balanced by a trim variable. For normal yachts this balance is achieved by increasing the heel angle φ which increases the righting moment from the keel and decreases the heeling moment from the sails. Increasing the heel angle of the AC75 however does not result in an increase in righting moment. Therefore, the moment must be balanced by a trim parameter controlling the forces from

164

the rig which is the sail´s *flat*-parameter τ. The pitching moment (m_y) of the AC75 can either be balanced by the pitch angle θ as with normal yachts or with the elevator rake δ_e. The elevator rake is constantly trimmed to maintain a target pitch angle and is hence better suited for balancing m_y as it better reflects the sailing style of the AC75.

Table 1: Different solver set-ups (state variables blue, trim variables grey).

	Conventional Yacht	AC75
f_x	boat speed V_S	boat speed V_S
f_y	leeway angle λ	leeway angle λ
f_z	sink d_z	flap angle δ_f
m_x	heel angle φ	flat τ
m_y	pitch angle θ	elevator rake δ_e
m_z	rudder angle δ_r	rudder angle δ_r
	Hooke-Jeeves	**Fixed targets**
	flat τ	heel angle φ
	crew x-position	pitch angle θ
	crew y-position	ride height (sink) d_z

The pitch angle as well as the ride height (sink) and the heel angle are however still relevant for solving the sailing state, but are fixed targets and must hence not be optimised. The target values were estimated from race data from America's Cup (2020). It suggests that the boats are on average pitched bow down by around 2°, heeled to windward by around 1.5° and fly 0.8 m above the waterline (this results in the hull being clear of the water by about 0.4 m). This fixing of state variables does mean a slight simplification of the problem but greatly increases the robustness of the routine as the optimisation loop using the Hooke-Jeeves algorithm can be neglected completely and only the Newton-Raphson method has to be employed. The resulting problem is expressed using Lagrange multipliers $(l_i \neq 0)$ within the functional

$$F = -V_S + l_0 \sum f_x + l_1 \sum f_y + l_2 \sum f_z + l_3 \sum m_x + l_4 \sum m_y + l_5 \sum m_z \,, \qquad (1)$$

where the first order condition for an extremum is

$$F \overset{!}{=} \ \min \ \rightarrow \ \nabla F \overset{!}{=} 0. \qquad (2)$$

This leads to a non-linear equation system with 12 equations:

$$f_0 = \frac{\partial F}{\partial V_S} \overset{!}{=} 0, \qquad f_1 = \frac{\partial F}{\partial \lambda} \overset{!}{=} 0, \qquad f_2 = \frac{\partial F}{\partial \delta_f} \overset{!}{=} 0,$$

$$f_3 = \frac{\partial F}{\partial \tau} \overset{!}{=} 0, \qquad f_4 = \frac{\partial F}{\partial \delta_e} \overset{!}{=} 0, \qquad f_5 = \frac{\partial F}{\partial \delta_r} \overset{!}{=} 0,$$

$$f_6 = \frac{\partial F}{\partial l_0} \overset{!}{=} 0, \qquad f_7 = \frac{\partial F}{\partial l_1} \overset{!}{=} 0, \qquad f_8 = \frac{\partial F}{\partial l_2} \overset{!}{=} 0,$$

$$f_9 = \frac{\partial F}{\partial l_3} \overset{!}{=} 0, \qquad f_{10} = \frac{\partial F}{\partial l_4} \overset{!}{=} 0, \qquad f_{11} = \frac{\partial F}{\partial l_5} \overset{!}{=} 0.$$

$$(3)$$

Using the following notation for the free variable vector

$$\boldsymbol{\xi} = (V_S, \lambda, \delta_f, \tau, \delta_e, \delta_r, l_0,\ l_1,\ l_2,\ l_3,\ l_4,\ l_5)^T, \tag{4}$$

the equation system in (3) can be written as follows:

$$f_i(\boldsymbol{\xi}) \overset{!}{=} 0 \quad \text{for } i = 0 \dots 11. \tag{5}$$

Using a Taylor expansion as approximation for f_i in the vicinity of a selected point $\sim\boldsymbol{\xi}_x$ and neglecting higher order terms yields a system of linear equations:

$$f_i(\boldsymbol{\xi}_x + \Delta\boldsymbol{\xi}) \approx f_i(\boldsymbol{\xi}_x) + \left.\frac{\partial f_i}{\partial \xi_0}\right|_{\xi_x} \Delta\xi_0 + \dots + \left.\frac{\partial f_i}{\partial \xi_{11}}\right|_{\xi_x} \Delta\xi_{11} \quad \text{for } i = 0 \dots 11, \tag{6}$$

where the partial derivatives of f_i are computed using a forward finite differencing scheme. In each iteration a correction is calculated and the procedure is stopped when a predefined accuracy is achieved, see Press et al. (1988) for more detail. A comparable approach was used by Patterson and Binns (2022), where the flap angle was balanced in a separate loop at every step of the Newton-Raphson.

2.2 FORCE MODULES

The forces of the AC75 are modelled with force modules for the gravitational forces, the aerodynamics of the sails and the hull, and the hydrodynamics of the foil, the rudder and the elevator. The gravity modules are used to model the forces and moments arising from the weight of the different components such as the hull and the crew. The weights of the components and crew were taken from the AC75 rule, while their lever arms were estimated from pictures. Inertia terms can be neglected completely for this stationary analysis.

Table 2. Projected areas, Centres of effort and Drag coefficients of the AC75 hull.

	Projected area [m²]	Centre of effort [m]	C_D
Front	7.4	8	0.25
Side	33.7	0	0.8
Top	79.8	0.5	0.8

The aerodynamic forces and moments arising from the hull are modelled with a simple force module based on drag coefficients in the three planes, the respective areas and centres of effort as shown in Table 2. The drag coefficients are taken from Hoerner (1965) for a comparable geometry whilst the areas and centres of effort are measured from a generic AC75 hull shown in the GUI of FS-Equilibrium in Figure 3.
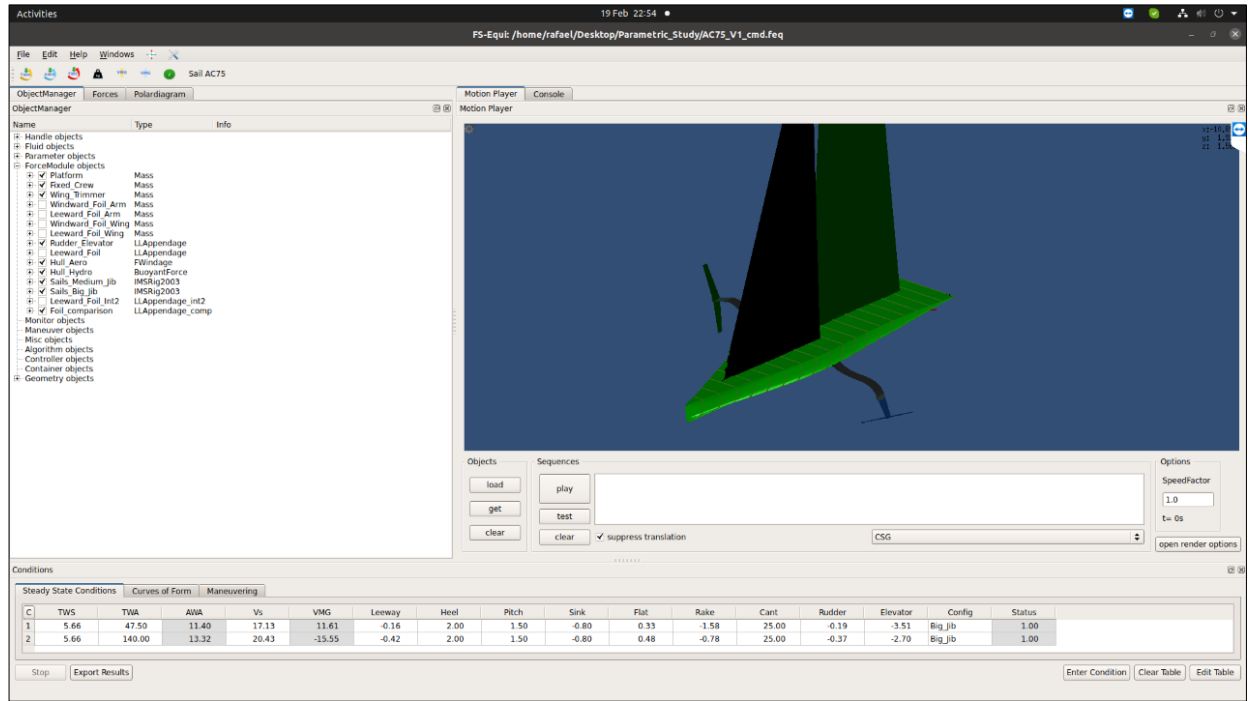
Figure 3. Graphical User Interface of FS-Equilibrium showing the employed hull.

The sail plan of the AC75 consists of several conventional jibs and a soft double skin mainsail both end-plated to the deck. The double skin mainsail is a complex component that enables trimming of the sheeting angle, the twist, and the depth and position of the large possible maximum camber in several locations along the span of the sail. The variable camber allows the generation of high lift coefficients which are used at take-off and deep true-wind angles in lighter winds. The end-plated double skin sail in combination with the rotating mast is also significantly more efficient than a conventional mainsail in general. In addition, the top of the mainsail can be inverted to generate righting moment. To capture these advanced features and trim possibilities a sophisticated sail model is under development. However at this stage, a simplified approach is taken by using the coefficient-based model for conventional rigs originated by Hazen (1980) presented below. The exact implementation follows that of the 2003 IMS VPP, that also accounts for the blanketing of the sails. A medium and a large Jib, in combination with the main sail, are modelled in so called 'configurations' and can be used according to the analysed conditions. The sail plan in this study corresponds to the sail plans of Luna Rossa, American Magic and INEOS Team UK which did not have the lower deck and extended luff like ETNZ. The details of the configurations are given in Table 3. The nominal area A_N is computed as the sum of the mainsail area A_M and the area of the foretriangle $A_F = 95.3 \text{ m}^2$.

Table 3. Configurations of the two sail plans

Configuration	Jib area A_J [m^2]	Main area A_M [m^2]	Nominal Area A_N	Aspect Ratio A_R
Medium Jib + Main	64.2	142	237.3	4.37
Big Jib + Main	74.4	142	237.3	4.37

Based on the sail areas and the force coefficients of the individual sails (Jib: C_{Lj} and C_{Dpj}, Main: C_{Lm} and C_{Dpm}), which are depending on the apparent wind angle β_a, the lift and drag coefficients (C_L and C_D) of the aggregate sail sets are computed with

167

$$C_L = \frac{C_{\text{Lj}} A_J + C_{\text{Lm}} A_M}{A_N} \tau \tag{7}$$

and

$$C_D = \frac{C_{\text{Dpj}} A_J + C_{\text{Dpm}} A_M}{A_N} + C_{\text{Di}}. \tag{8}$$

C_{Di} is the induced drag coefficient:

$$C_{\text{Di}} = C_L{}^2 \left(\frac{1}{\pi A_R} + 0.005 \right), \tag{9}$$

where the aspect ratio is

$$A_R = \frac{(1.1 (E_{\text{HM}} + F_A))^2}{A_N}. \tag{10}$$

E_{HM} is the mast height above the shear line and F_A is the average freeboard height, both in meters. For more detail see Larsson et al (2014) and Molland et al (2017). The aggregated coefficients are given in Figure 4 as a function of the apparent wind angle and are then transformed into the driving force coefficient

$$C_R = 1.3 \left(C_L \sin(\beta_a) - C_D \cos(\beta_a) \right), \tag{11}$$

and the heeling force coefficient

$$C_H = C_L \cos(\beta_a) + C_D \sin(\beta_a). \tag{12}$$
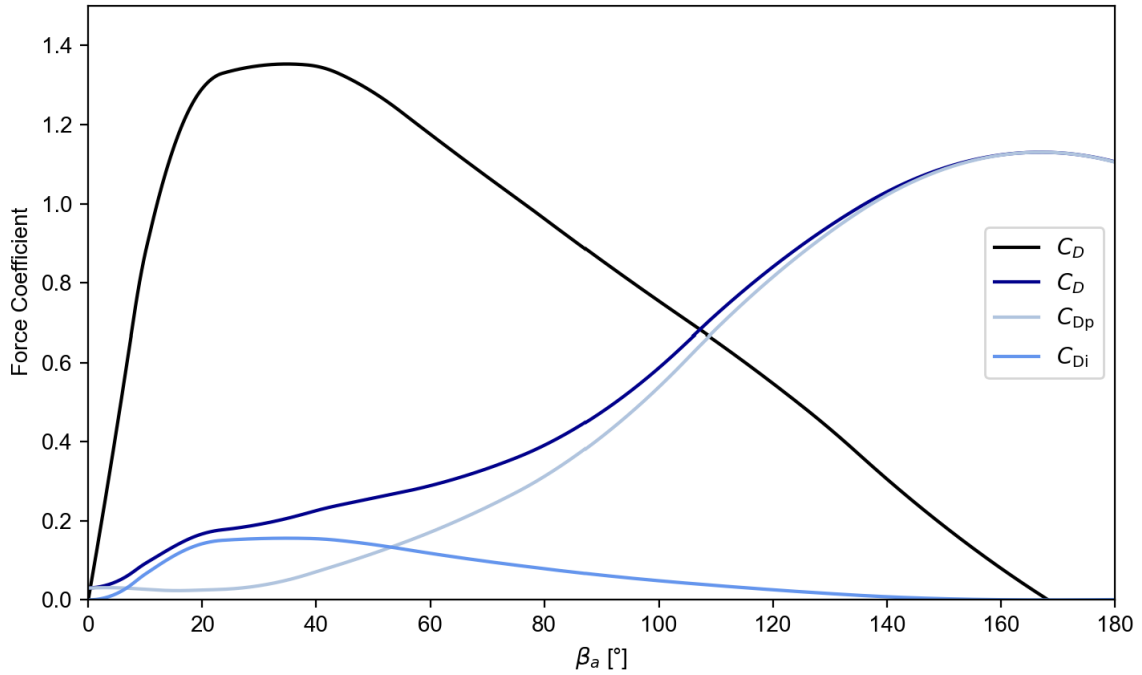
Figure 4. Aggregated lift and drag coefficients of the configuration "Medium Jib + Main".

As the forces predicted by the IMS model do not account for the increased efficiency due to the end-plated main, the rotating mast and the double skin sail, a factor on the driving force is included. According to Bergstrom and Ranzén, reported in Larsson et al (2014), the lift coefficient of a sail with a gap between the boom and the deck of 7% of the mast height leads to a 22% increase in drag coefficient and a decrease in lift coefficient of 13% compared to an end-plated sail. For an AC75-typical apparent wind angle of 13°, this results in a 20% gain in driving force due to end-plating. A significant additional performance increase is expected due to the rotating mast and double skins, not to mention the more advanced trimming possibilities. Therefore, a factor of 1.3 is applied to the driving force as shown in Equation 11. This achieves accurate results on most courses as presented in Section 5.

3. HYDRODYNAMIC FOIL MODEL

The forces and moments generated by the hydrofoil of the AC75 are modelled using an advanced lifting line method based on the formulation of Phillips and Snyder (2000) as summarized by Reid (2020). In contrast to the original lifting line method by Prandtl (1918), the approach employs horseshoe vortices at every station along the span and a vectorised form of the Kutta-Jukowski-Law. Every horseshoe vortex consists of a bound vortex and two semi-infinite vortices. The semi-infinite vortex sheet is oriented in the negative x-direction, so opposite to the direction of travel. The control points are located in the middle of every segment at quarter chord. Employing the vectorised lifting law includes the influence of the bound vortices on each other which is required to correctly model the effects of leeway, sweep or anhedral. Furthermore, it enables modelling the influence of multiple wings on each other. The method solves for the strength of each horseshoe vortex Γ_j by relating two definitions of the force generated per segment. The force generated by every bound vortex is calculated from

$$\mathrm{d}\boldsymbol{F_i} = \rho \Gamma_i \boldsymbol{V_i} \times \mathrm{d}\boldsymbol{l_i}, \tag{13}$$

where the local velocity at each control point is computed with

$$\boldsymbol{V_i} = \boldsymbol{V}_\infty + \sum_{j=1}^{N} \Gamma_j \, \boldsymbol{v}_{\mathbf{ji}}, \tag{14}$$

where $\boldsymbol{v}_{ji}$ is the induced velocity of horseshoe vortex j at control point i normalised by the vortex strength. Relating the vectorised vortex lifting law to a definition of the lift based on the sectional lift coefficient results in a non-linear system of equations which is solved iteratively. Due to the non-linearity, the method can account for the effects of stall, but is potentially unstable. Therefore, the approach was reduced to a linear problem by applying a linear lift-curve slope to increase robustness and reduce computational time. This yields the linear system of equations

$$\rho \Gamma_i \left| \left(\boldsymbol{V}_\infty + \sum_{j=1}^{N} \Gamma_j \, \boldsymbol{v}_{\mathbf{ji}} \right) \times \mathrm{d}\boldsymbol{l_i} \right| - \frac{1}{2} \rho \boldsymbol{V}_\infty^2 \, C_L(\boldsymbol{V_i}) \mathrm{d}A_i = 0. \tag{15}$$

For a more general introduction to lifting line methods and other numerical models for hydrofoils see Molland and Turnock (2021). Each part of the hydrofoil is discretised using 40 segments with a cosine-distribution as recommended by Phillips and Snyder (2000) for the best trade-off between accuracy and computational time. The parts of the hydrofoil that are above the waterline are `cut off´ and not included when computing the forces (Figure 5).
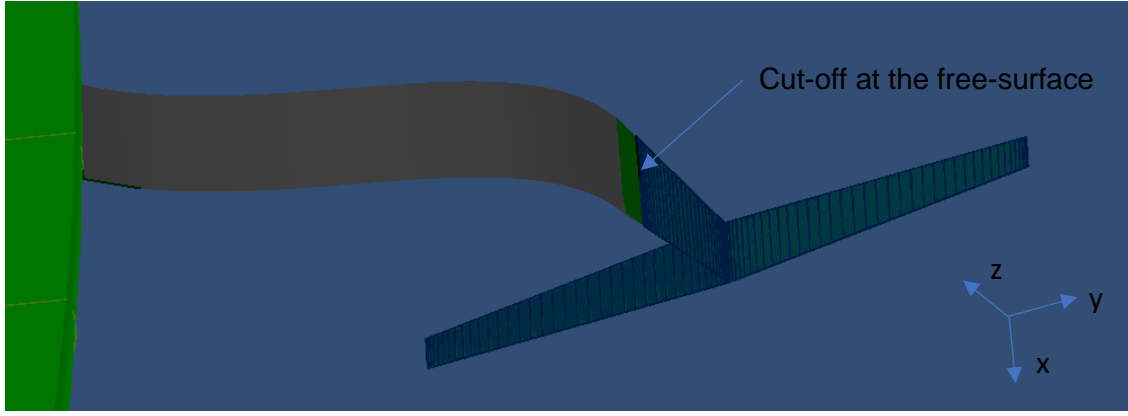
Figure 5. AC75 foil discretised with 40 stations per foil part and cut-off at the free-surface.

The loss in lift due to the free surface is modelled using a second transformed foil according to the biplane analogy (Faltinsen, 2005) shown in Figure 6(a). The analogy is applicable if the submerged Froude number

$$F_{Nh} = \frac{V_S}{\sqrt{gh}} \tag{16}$$

is higher than $10/\sqrt{h/c}$, where V_S is the velocity, g the gravitational field strength, h the submersion and c the chord. For the average tip chord in the study $c = 0.25$ m and the submersion of the outboard wing at the tip $h \sim 0.25$ m ($h/c = 1$), the required minimum submerged Froude number is 10. The actual submerged Froude number for the average boat speed in the study $V_S = 19$ m s^{-1} is 12.13 at the outboard tip and therefore satisfies the criterion. At the root of the half wing, where the average submersion is 0.82 m and the average chord is 0.6 m ($h/c = 1.37$), the criterion of 8.54 is not satisfied ($F_{Nh} = 6.69$), but the effect of the free-surface is smaller due to the higher h/c ratio (see Figure 6(b)). More importantly, the loss in lift prior to the required submerged Froude number is even higher, so there is no harm in applying the biplane-image as long as F_{Nh} does not tend to zero. Close to $F_{Nh} = 0$, the lift is increased due to the free-surface, but such low Froude numbers were not experienced in the study.
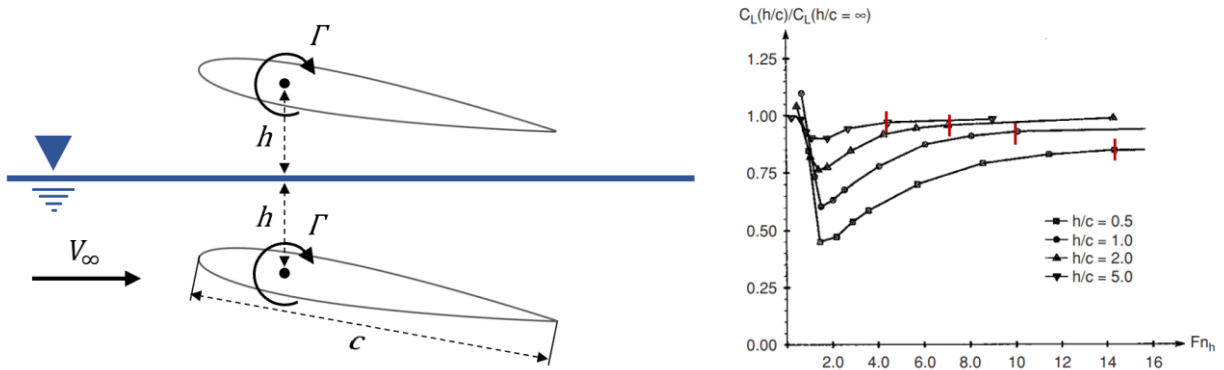

Figure 6. (a) Biplane transformation around the free-surface plane; (b) Change in lift coefficient as function of the submerged Froude number for different h/c-ratios, red bars represent $F_{Nh} = 10/\sqrt{h/c}$; Derived from Faltinsen (2005).

The sectional lift coefficient at every station is computed from the lift-curve-slope and the zero-lift-angle. The zero-lift-angle is provided in the form of a response surface as a function of the flap angle

170

and the span s of the foil using a sequential interpolation based on C-splines. Similarly, the sectional profile drag coefficient per station is computed from a response surface depending on the flap angle, the Reynolds number, the lift coefficient and the span. The response surface is based on an inverted distance weighting function. The underlying data of both surfaces was computed using viscous XFoil simulations. For the extension of the foil arm, which has to be symmetric according to the AC75 rule, a NACA 0008 section was used while the foil wings have an asymmetric Eppler 874 hydrofoil section. Figure 7 shows the two response surfaces of the Eppler 874 section with the corresponding data points. The green colour indicates a fitting error below 1%. The range of points is chosen such that the AC75 foil will operate in this range at all times. Wave-making drag, spray drag and junction drag are not/not yet considered.
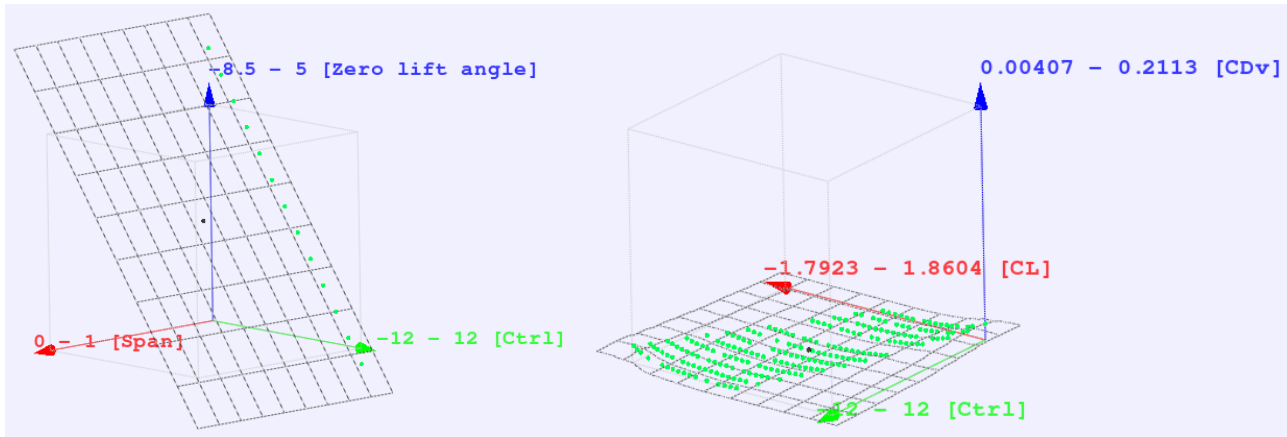

Figure 7. Response surfaces for the Eppler 874 section, zero-lift-angle (a), sectional profile drag C_{Dv} (b) at $Re = 3 \times 10^7$ and $s = 0$; Ctrl corresponds to flap angle.
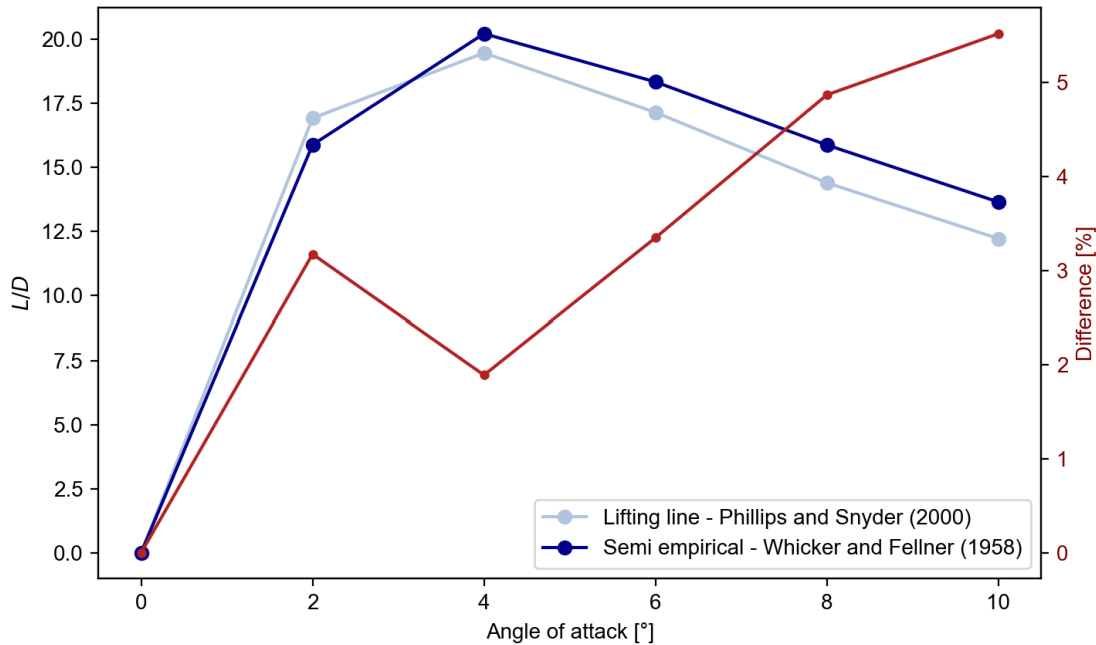

Figure 8. Comparison of lift to drag ratios (L/D) as a function of angle of attack computed by the advanced lifting line method and Whicker and Fellner (1958) at $Re = 1.8 \times 10^6$.

The advanced lifting line method is validated with the semi empirical equations for low-aspect-ratio foils presented by Whicker and Fehlner (1958). The chosen geometry has an aspect ratio of 3, a taper ratio of 0.45 and 0° sweep at the quarter chord line. A NACA0015 section is used with no twist

along the span. Figure 8 shows the resulting lift to drag ratios as function of the angle of attack plus the difference of the two models. It shows that the difference is usually below 5% and only exceeds it at 10° angle of attack.

The lifting line method returns the hydrodynamic forces and moments generated from the lifting surfaces. Additionally, the force module computes the weight of the current foil design based on a weighted average density of 8305 kg m^{-3} of the involved materials (75% high density steel, 20% lead and 5% hydraulic oil to represent the control systems). If the foil design does not meet the required 921 kg, an ellipsoidal bulb is automatically sized to meet the requirement. If the foil is exceeding the required weight, it is marked as too heavy. The module also computes the gravitational forces and moments of the foil which are added to the hydrodynamic forces. The centre of gravity of the foil is hereby computed based on the current design. If a bulb is included, the additional hydrodynamic drag is computed using a form factor approach (Equation 17). The frictional resistance Rf is calculated from the area of the bulb and the friction drag coefficient derived from the ITTC line (Specialist Committee of 23rd ITTC, 2002). The form factor $(1 + k)$ is computed based on the chord c and the thickness t of the bulb according to Equation 18. The bulb drag and the corresponding moments are added to the forces and moments computed previously and returned to the Newton-Raphson method as a whole. Very small bulbs might lead to a slightly lower overall drag opposed to an increased drag as they reduce junction drag, this however cannot be modelled with the lifting line method.

$$R_T = R_F(1 + k) \tag{17}$$

$$(1 + k) = 1 + 2\frac{t}{c} + 60\left(\frac{t}{c}\right)^4 \tag{18}$$

4. PARAMETRIC MODEL

The parametric model of the hydrofoil serves to generate the shape of a hydrofoil from a set of design variables. The foil geometry is provided to the lifting line method in the form of 'ruled surfaces' which are based on NURBS surfaces. NURBS surfaces are defined as

$$S(u, v) = \frac{\sum_{i=0}^{n} \sum_{j=0}^{m} N_{i,p}(u) N_{j,q}(v) w_{i,j} P_{i,j}}{\sum_{i=0}^{n} \sum_{j=0}^{m} N_{i,p}(u) N_{j,q}(v) w_{i,j}} \quad \text{for } 0 \le u, v \le 1, \tag{19}$$

where $P_{i,j}$ are the control points, u and v the directions alongside the surface (u spanwise, v chordwise) and p and q are the degrees in the u- and v-direction, respectively. $N_{i,p}(u)$, $N_{j,q}(v)$ are the nonrational B-spline basis functions and $w_{i,j}$ are the weights of the control points. For more detail see Piegl and Tiller (1997).

From the NURBS surfaces the lifting line method derives the relevant geometrical information such as the chord and the twist along the span of the foil. Figure 9 on the left shows an AC75 foil described by 86 input variables which are used to generate the underlying NURBS surfaces developed as part of this research. This sophisticated model is detailed enough to re-create the shapes of the hydrofoils seen in the 36th America's Cup. Two of which are shown in Figure 9 on the right representing geosims of the ETNZ (upper) and Luna Rossa (lower) foils, respectively. Although very complex foil shapes can be generated, the sheer number of input variables makes it impossible to examine parametrically. This sophisticated parametric model will be used in an adjoint optimisation in the future that allows the optimisation of hundreds of design variables in a very effective manner.
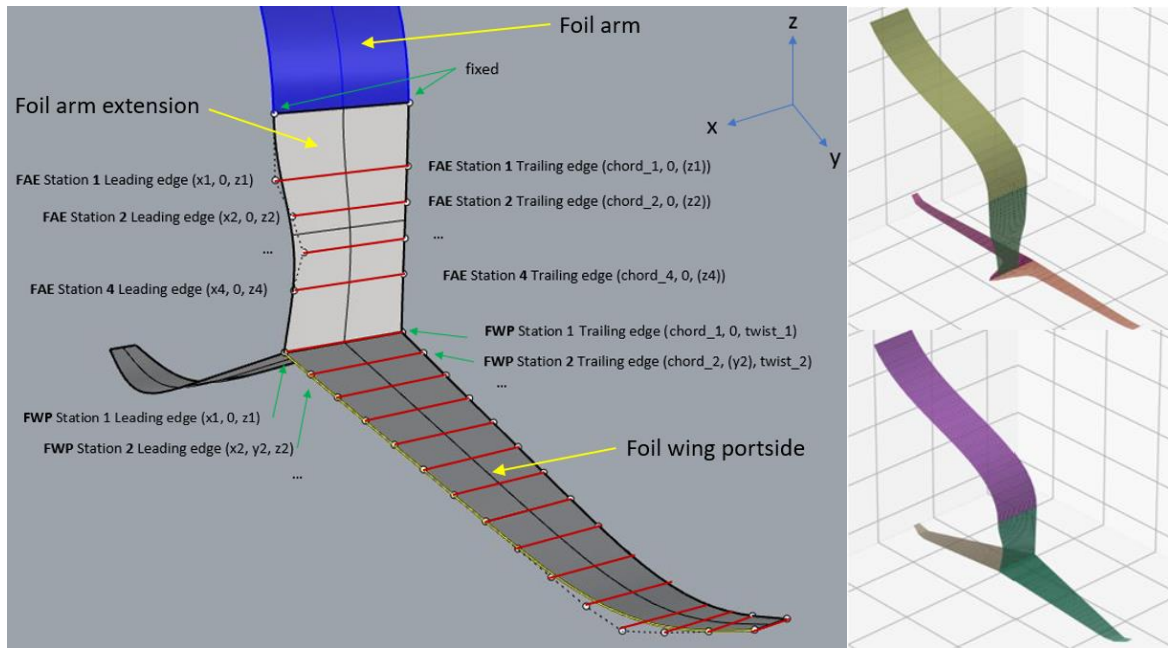
Figure 9. NURBS-based parametric model of the AC75 foil using 86 design.

For the purposes of this paper however, a simplified NURBS-model was developed which is defined by 6 points (each with a x, y and z-coordinate) as shown in Figure 10. These 18 variables are computed from the variables extension length, semi span, root chord, taper ratio and wing rake which are examined in the parametric study to further simplify the problem and to enhance the readability of the results. The model exploits the symmetry requirements, which means that the portside half wing is mirrored to define the points of the starboard half wing. The z-position of the wing tips is fixed on the bottom of the foil box to enable the definition of the spine form with just the extension length and the semi span. Winglets are not considered. Both parametric models are based on the C++ library TinyNURBS (Jayaraman, 2022) and use the python library NURBS-python (Bingol, 2022) for visualisations. The parametric model is coupled to the lifting line method internally for increased computational efficiency and user-friendliness.
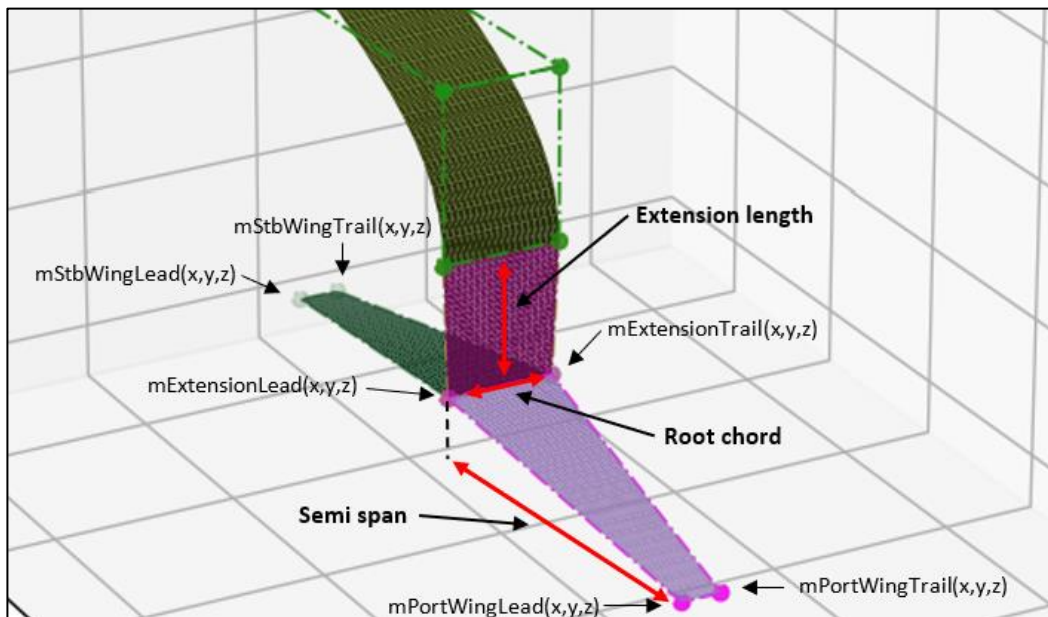

Figure 10. Simple parametric model of the AC75 hydrofoil showing the control points employed to define the hydrofoil geometry.

5. VPP VALIDATION

The AC75 VPP model is validated with real live data recorded during the last America's Cup (America´s Cup, 2020). Ten races were sailed in light to moderate conditions, of which three races are selected to cover this range. In race one the average wind speed was around 13 kts, while races three and seven were sailed in 9 and 11 kts, respectively. From these three races, situations were chosen where both teams (ETNZ and Luna Rossa) sailed in comparable conditions. This means that there were no visible differences in wind speed and that the yachts were far enough apart to not interfere with each other. Per race, four such situations are selected, two sailing upwind and two sailing downwind. The results are presented in Table 4, where true wind speed V_{TW}, boat speed V_S and velocity made good V_{MG} are given in knots and the true wind angle β_t is presented in degrees. In addition to the V_{MG} measured at the specified time, the variation in V_{MG} in a ten second window is provided in brackets. For comparison, two foils similar to those of ETNZ and Luna Rossa were modelled and tested. The designs are based on the simplified parametric model so they do not perfectly represent the details of the real foils, but they do have the similar root chords, taper ratios and anhedral angles. The hull, the sail plan and the remainder of the yacht are however not altered. The velocity polars of the two foils are computed for the true wind speeds 9, 11, and 13 kts. A macro is defined in FS-Equilibrium that initiates the force balance and plots the polars for every wind speed. The larger jib is used in 9 and 11 kts V_{TW}, while the medium sized jib is used in 13 kts.

Table 4. America's Cup race data from ENTZ and Luna Rossa.

Race	Time	ETNZ				Luna Rossa			
		V_{TW} [kts]	V_S [kts]	V_{MG} [kts]	β_t[°]	V_{TW} [kts]	V_S [kts]	V_{MG} [kts]	β_t[°]
1	01:27	13	36	24 (22 - 25)	48.2	13	34	24 (24 - 27)	45.1
	01:50	14	38	27 (26 - 27)	44.7	14	36	24 (24 - 26)	48.2
	13:31	13	42	35 (34 - 36)	146.4	13	42	36 (34 - 36)	149
	21:14	13	43	37 (36 - 37)	149.4	13	43	36 (34 - 36)	146.8
3	02:29	8	33	21 (20 - 22)	50.5	9	30	17 (16 - 20)	55.5
	11:57	9	33	19 (19 - 22)	54.8	10	29	15 (12 - 21)	58.9
	06:08	10	38	30 (29 - 30)	142.1	10	35	27 (27 - 28)	140.5
	16:28	9	36	31 (29 - 32)	149.4	10	36	27 (26- 28)	138.6
7	02:30	11	36	24 (23 - 25)	48.2	11	32	21 (17 - 21)	54.5
	09:30	11	32	24 (21 - 24)	41.4	11	31	22 (18 - 23)	44.8
	05:42	11	40	34 (33 - 35)	148.2	11	40	28 (27 - 29)	134.4
	15:10	11	42	33 (33 - 34)	141.8	11	42	30 (28 - 30)	135.6

Figure 11 shows the velocity polars for both yachts which also include the measured points from Table 4 (single points with red edging). Firstly, it can be seen that all velocity polars are smooth curves which suggests a very robust solver set-up. Secondly, the presented polars for 11 kts V_{TW} show very good agreement of the predicted and the measured performances. This is also true for the polars in 13 kts. The polar of Luna Rossa in 9 kts shows excellent agreement on upwind courses but is underperforming in the downwind cases. This can be explained by the use of the IMS sails aero module which does not model the high achievable camber of the double skin main sail. This feature allows the generation of high lift coefficients and hence high drive forces, beneficial in these conditions. This effect is less visible at higher wind speeds or when sailing upwind, where the boats are operated with less camber. The polar of ETNZ in 9 kts V_{TW} is underperforming on all courses which can be explained by the sail plan which is based on those of the challengers and does not have the extended sail area the ETNZ boat had in reality. This extended sail area is assumed advantageous at low wind speeds. The discrepancy on downwind courses is higher which

is again due to not modelling the deep camber. Similar trends were observed by Patterson and Binns (2022).
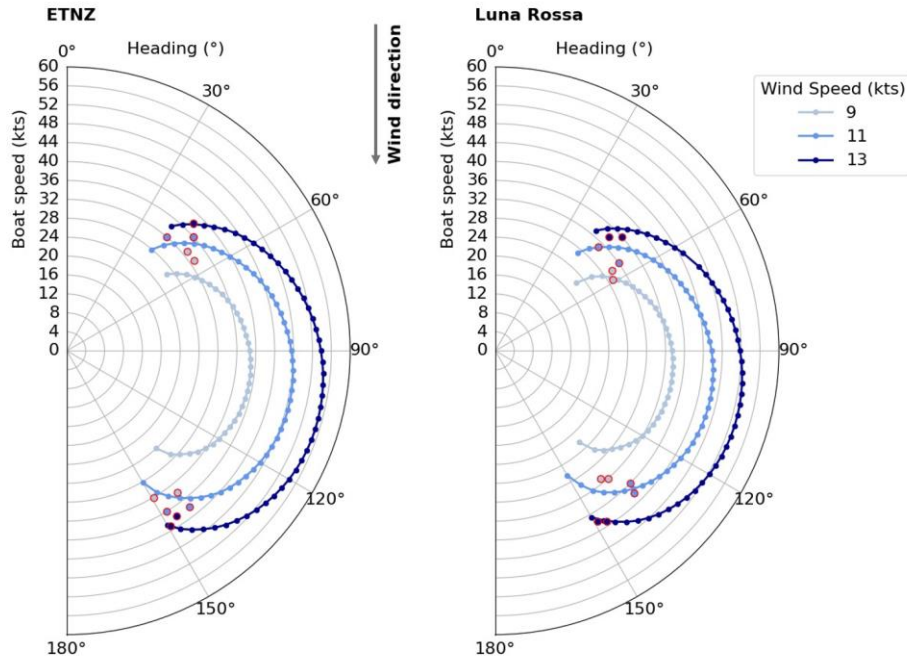

Figure 11. Velocity polars of the two foil designs of ETNZ and Luna Rossa compared to the real life data points from Table 4 (points with red edging).

While the generated polars show very good agreement with the measured data, they are still heavily influenced by the tuning of the aerodynamic model of the sails (factor of 1.3 on driving force) which introduces uncertainty. They also lack in perfectly modelling downwind performance. As a consequence the development of an aerodynamic sails model that can reflect the AC75 sails accurately is part of current work. The module will be based on a machine learning model trained with a panel code.

6. PARAMETRIC STUDY

The parametric study examines the foil design parameters extension length, semi span, root chord, taper ratio and wing rake. The spine form of the foil is defined with the extension length and the semi span while the plan form of the foil is specified with root chord and taper ratio. The fixed rake of the wing is defined by the wing rake variable. The study is carried out for any combination of the variable values specified in Table 5. The parameter set-up and the values are chosen to maximise the understanding of the parameters, while keeping the number of required simulations as low as possible. The range of variable values results in a total of 72 design candidates. The simple parametric model originally also incorporated a variable to define the sweep of the foil. However, initial results have shown that any amount of sweep is reducing the performance of a design compared to its non-swept version. Therefore, this variable was excluded for the sake of simplicity. The performance of all candidates is evaluated on up- and downwind courses in three different wind speeds, 8, 11 and 14 kts V_{TW}, best representing the range of conditions recorded during the last America´s Cup. The courses sailed in the up- and downwind conditions are selected according to the courses that resulted in the highest V_{MG} in Section 5. The leeward foil is canted out by 25° to maximise righting moment while being just fully submerged. Running the study was automated using a python script and the batch mode of FS-Equilibrium.

Table 5. Parameter values

Parameter	Values
Extension length	600 mm, 950 mm, 1300 mm
Semi span	1750 mm, 1880 mm
Root chord	400 mm, 800 mm
Taper ratio	0.25, 0.5
Wing rake	0.0°, 2.0°, 4.0 °

6.1 RESULTS

Figures 12 and 13 show the up- and downwind performances of the 72 foil candidates in 11 kts V_{TW}. Figure 14 presents the upwind performance in 8 kts V_{TW}, the slowest of the assessed conditions, and Figure 15 the downwind performance in 14 kts V_{TW}, the fastest condition. The legend of the figures can be used to determine what spine and planforms the candidates have. These are defined by the extension length, the semi span, the root chord and the taper ratio. The figures show three candidates within every taper ratio band. These three designs share the same spine and planforms but have different wing rakes. The first candidate within every band has a wing rake of 0.0°, followed by the rakes 2.0° and 4.0°. If a point is not shown, no foiling equilibrium could be found. All foils weigh exactly 921 kg.
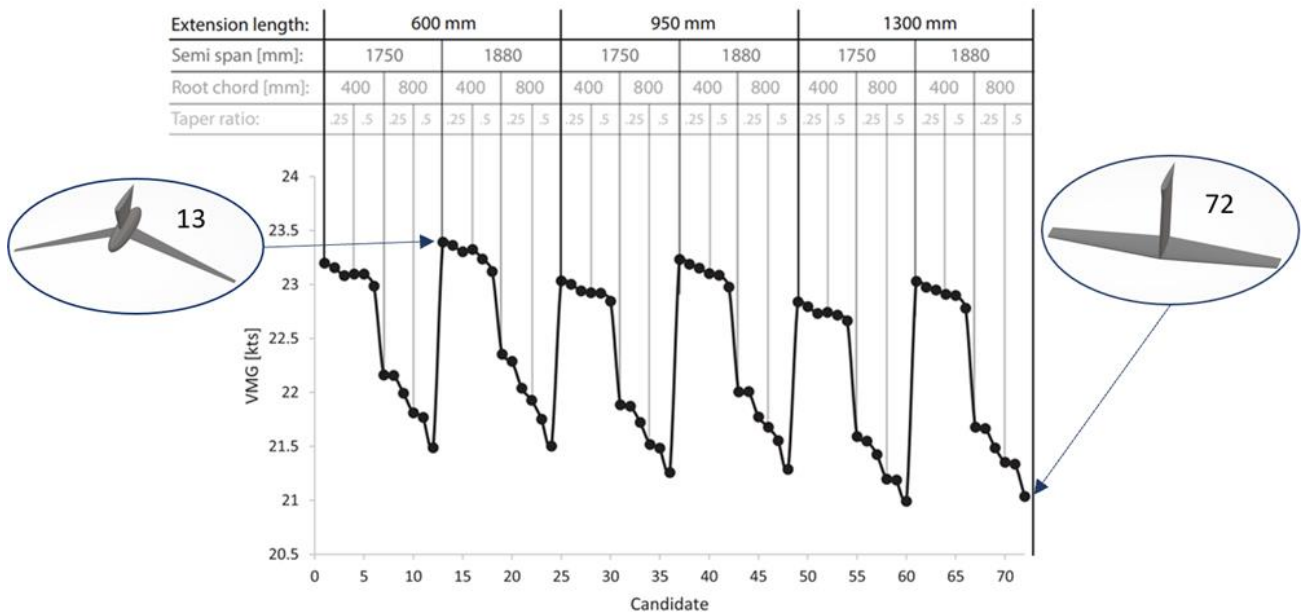

Figure 12. Foil performance in 11 kts upwind at $\beta_t = 47.5°$.

Figures 12 and 13 show that foils with lower extension lengths and hence higher anhedral angles perform better than foils with higher extension lengths. This is true for up- and downwind conditions in all three evaluated wind speeds (see also Figures 14 and 15) and can be explained by two effects. Firstly, the extension of the foil is mainly only used to connect the arm and the wing and is not actively employed to generate side force or vertical lift. Therefore, it is better to store the required weight in a larger wing that is then operated at a lower wing rake or flap angle or in the bulb which has a lower wetted surface area for the same volume. Storing the required weight in a longer extension only causes additional drag. Secondly, the foils with higher extension length generally have a longer spine than the same foils with lower extension. Having a fixed volume, the components are therefore automatically longer and more slender, which means that their ratio of wetted surface area to stored weight is higher.
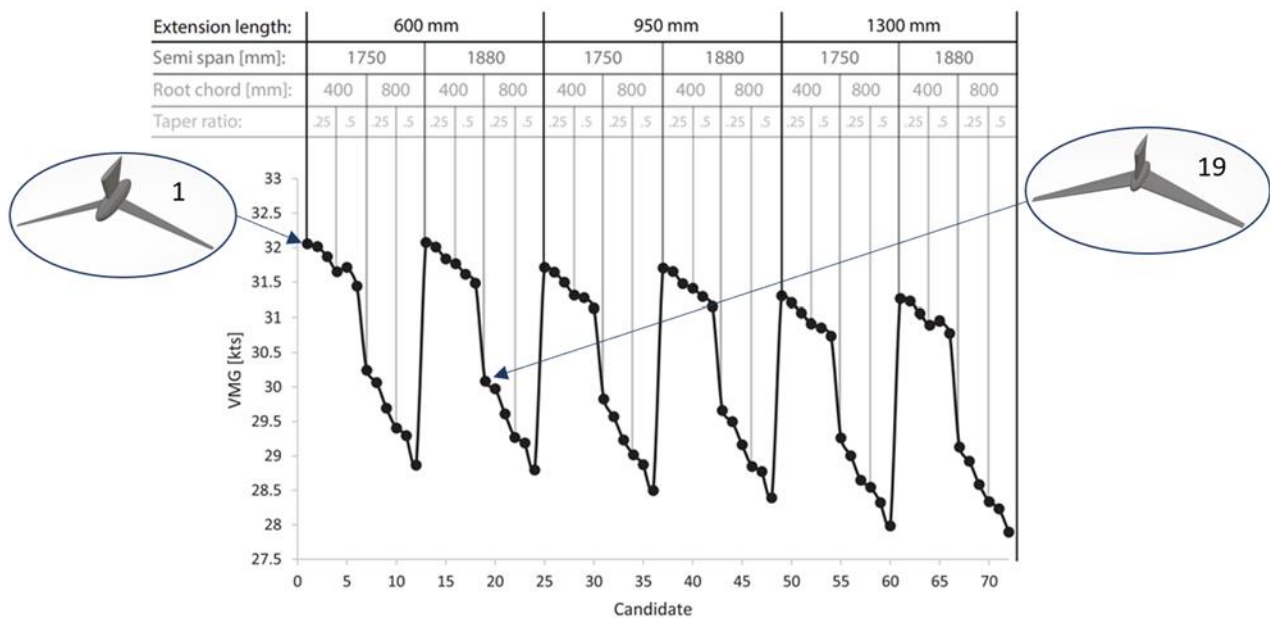
Extension length:	600 mm								950 mm								1300 mm							
Semi span [mm]:	1750				1880				1750				1880				1750				1880			
Root chord [mm]:	400		800		400		800		400		800		400		800		400		800		400		800	
Taper ratio:	.25	.5	.25	.5	.25	.5	.25	.5	.25	.5	.25	.5	.25	.5	.25	.5	.25	.5	.25	.5	.25	.5	.25	.5

Chart: VMG [kts] (y-axis, 27.5 to 33) vs Candidate (x-axis, 0 to 70). Callout 1 at the left, callout 19 at the right.

Figure 13. Foil performance in 11 kts downwind at $\beta_t = 140°$.

A further benefit of the foils with anhedral angle is that the two flap segments (one on each half wing) can be used independently. When the foil is canted out, the ride height can be adjusted with the flap of the almost horizontal outboard half wing and the leeway angle can be controlled with the flap of the almost vertical inboard half wing. Furthermore, it also allows to shift the centre of effort further outboard, and hence to increase the righting moment generated by the foil. However, these effects cannot yet be reflected in the AC75 VPP model. Nevertheless, a shorter extension also means that the outboard side of the wing operates closer to the free surface when canted out compared to a higher extension foil. This does reduce the lift generated and increases the drag due to wave-making. It potentially also promotes cavitation and ventilation. The reduced lift is modelled using the biplane image, which is best suited for the design space and conditions explored, and seems to not outweigh the benefits of the high anhedral angle. Wave-making drag and potential cavitation and ventilation are not included. This means that in reality a foil with medium extension could outperform the lowest extension foil and could be an explanation why the three challengers in the America´s Cup with Y-foils did not chose to have the highest possible anhedral angle. Another explanation could be that the constraint on centre of gravity in the AC75 rule is active above a certain anhedral angle.

The semi span of the foil influences both the planform area of the foil and the aspect ratio. At lower boat speeds such as sailing upwind in 11 kts and up- and downwind in 8 kts V_{TW} the higher semi span performs better as it reduces the dominant induced drag (Figures 12 and 14). At higher boat speeds (sailing downwind in 11 kts and up – and downwind in 14 kts V_{TW} , Figures 13 and 15) the slightly lower span performs better. In these conditions the profile drag is dominant which can be reduced by decreasing the area of the foil. This outweighs the higher induced drag caused by the lowered semi span. A foil where the root chord would be further reduced instead of the semi span would however still perform better, as it would reduce viscous drag while keeping induced drag constant.

The root chord has the highest influence on the yacht´s performance in this study. This can be partially explained by the high difference between the root chord values, especially compared to the values of the semi span. It is however also caused by the large effect of the root chord on the area of the foil, as it also influences the tip chord via the taper ratio. The smaller root chord performs significantly better in 11 and 14 kts and going downwind in 8 kts V_{TW} due to the significantly lower area (Figures 12, 13 and 15). This also applies to most candidates in the slowest condition (sailing upwind in 8 kts V_{TW}, Figure 14). However, some candidates (Candidates 2, 26, 42, 49, 50, 51 and 62) cannot support the weight of the yacht in this condition due to their low planform area, especially

if they also have the lower semi span and the lower taper ratio. As the foil must be able to support the yacht in even slower conditions such as during take-off or during a tack and the span is limited by the rule, the root chord has to be chosen carefully and should not be too low. The root chord is also relevant to structural aspects which are not yet considered.
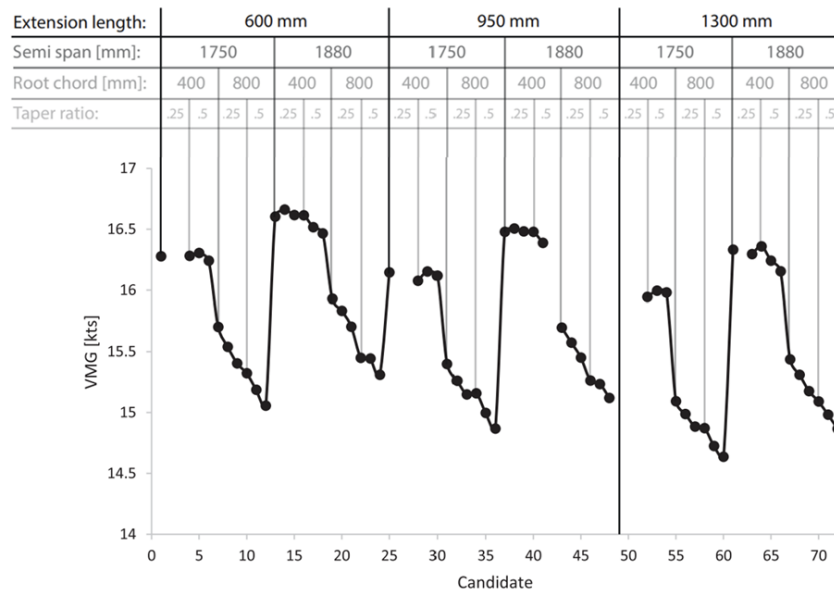

Figure 14. Foil performance in 8 kts upwind at $\beta_t = 57.5°$.

The taper ratio also influences the area of the foil but less significantly than the root chord as it only affects the tip chord. Generally, the smaller taper ratio leads to higher V_{MG} as the foils do not require the larger area in most conditions. The weight is better stored in the bulb which has a lower wetted surface area to weight ratio. An exception are the candidates with the smaller taper ratio of those mentioned above, that could not support the weight of the yacht anymore.
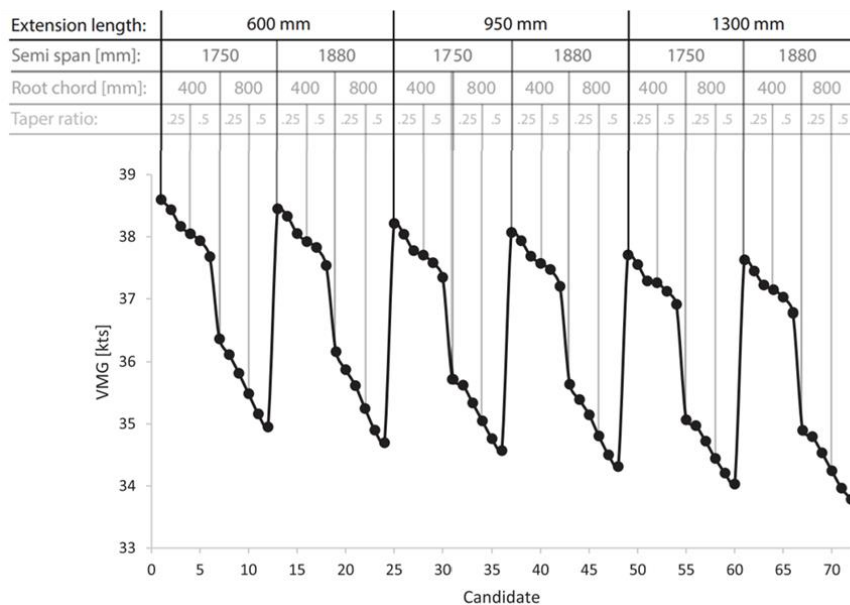

Figure 15. Foil performance in 14 kts downwind at $\beta_t = 140°$.

The wing rake of the hydrofoil determines the angle of attack at every section, where a higher rake results in higher lift forces. To control the amount of lift generated, the crew uses the flap angle which can be trimmed actively. The results show that the foils with the lowest rake (0.0°) perform best in most conditions. The Eppler 874 section has a zero lift angle of -0.5°, so the foil is generating positive lift at 0.0° rake even if the flap is not actuated. The amount of lift produced without the flap engaged is however not sufficient to support the weight of the yacht. Candidate 13 with 0.0° rake for example is operated at a flap angle of 8° in 11 kts V_{TW} upwind. Candidates 14 and 15 with the higher rakes are operated at 5.6° and 3.1° flap angle, respectively and are slower than Candidate 13. This shows that the foils with lower rake angles and higher flap angles are more efficient. This is true for all conditions assessed except the upwind condition in 8 kts V_{TW}. Here candidate 13 with a rake of 0.0° and a flap angle of 10° is performing less than candidate 14 with 2.0° rake and 7.4° flap angle. This suggests that too high flap angles reduce efficiency again. To increase the efficiency of candidate 13 at low boat speeds, the yacht could be sailed at a lower bow-down pitch, which would reduce the required flap angle.

The study has shown that candidate 13 with the shortest extension, the larger span, the smaller root chord and taper ratio and the smallest rake performs best across the range of conditions. The worst performing design is candidate 72, the T-Foil with high semi span, high root chord, high taper ratio and highest rake. Candidate 13 is on average 13.3% faster than candidate 72 and shows the immense influence of hydrofoil design on performance. However, while candidate 13 is performing best in the assessed conditions, it might have a too low planform area to support the yacht during take-offs and tacks. This would render the foil unsuitable and shows that at least one such condition should be included in the design process. Including such a condition would potentially favor Candidate 19, the best performing foil among the designs with higher root chord. Ultimately, also the weighting of the assessed conditions has a huge influence on the design. A higher weighting of the faster conditions for example could have favored candidate 1 with the lower semi span.

6.2 PARAMETRIC STUDY RESULTS VS REAL LIFE OBSERVATIONS

In contrast to the trends observed in the parametric study, the 36th America´s Cup has shown that ETNZ with their T-Foil was faster than the challengers with their Y-Foils. While this can partially be caused by other components of the yacht, such as the larger sail plan of ETNZ or the different hull which is not reflected in this study, it is supposedly also driven by the hydrofoil design. The study has assumed that the foil is fully submerged at all times with the outboard tip of the wing just operating below the free surface. This is a valid assumption for the foils of the challengers that have been operated fully submerged. ETNZ however employed their foil as a surface piercing foil at higher boat speeds which allowed the reduction of wetted surface area when not needed. The parametric study has shown similar trends, as the foils with lower span performed better in high speed conditions. In surface-piercing operation, the T-foil is assumed superior as the angle at which it pierces the surface is larger which reduces the risk of ventilation. While the operation as a surface piercing foil can be modelled with the developed VPP model, it would require the introduction of the cant angle as another parameter of the study with relatively many values. The parametric examination of the cant angle is therefore not feasible, but its optimisation will be part of the adjoint hydrofoil optimisation routine currently under development. Moreover, the model cannot account for ventilation which would probably result in the Y-Foils still being favored in the surface piercing mode. In addition, ETNZ has used a single control system to actuate both flaps simultaneously. This meant that they could not change the direction of the force vector anymore, but allowed them to remove one control system which reduced the required volume and associated wetted surface area. This is not reflected in this study, which assumed a constant density. The performance results have shown a high sensitivity to wetted surface area and hence both effects are expected to have a significant influence. Finally, the foil benefitted from its low chord which is in line with the findings of this study.

7. CONCLUSIONS

Hydrofoils are the biggest performance differentiators on sailing yachts like the AC75 and have a significant influence on the performance and the sailing state of the yacht. However, they are mostly designed and optimised in terms of their lift and drag characteristics which do not directly reflect the performance of the yacht on the race course. Therefore, a physics model of the AC75 has been developed in the VPP FS-Equilibrium and used to assess the effects of the main hydrofoil design variables on the performance of the yacht in different conditions. The results showed that the candidate with the shortest extension, the longer span, the smaller root chord and taper ratio and the lowest rake performed best across the range of conditions. Furthermore, the results have shown how valuable the VPP driven approach is as it allows the direct and accurate comparison of the candidates in terms of their performance on the race course.

While the parametric study is helpful to identify the trends in foil design it is not suitable for detailed optimisation as it would require a prohibitively expensive amount of VPP simulations. Therefore, a VPP driven gradient based optimisation strategy is proposed as shown in Figure 16. Gradient based optimisation is deemed significantly more efficient than parametric studies and gradient free optimisation. The straight forward way to compute a gradient is the finite difference method where each input variable is slightly perturbated, one at a time, to approximate its influence on the V_{MG}. This is a valid for optimising smaller numbers of variables. However, to approximate a single gradient of the advanced parametric model shown in Figure 9 with 86 design variables, 87 VPP simulations would be required. This is again too expensive. For cases with such a high number of input variables the only feasible method to compute the gradient is the adjoint method. This method allows to compute the gradient at the run time of just a handful of VPP simulations independent of the number of input variables. Therefore, it enables the optimisation of thousands of design variables and hence very detailed design in a short time. This adjoint VPP is currently under development and has achieved promising results in first optimisations.
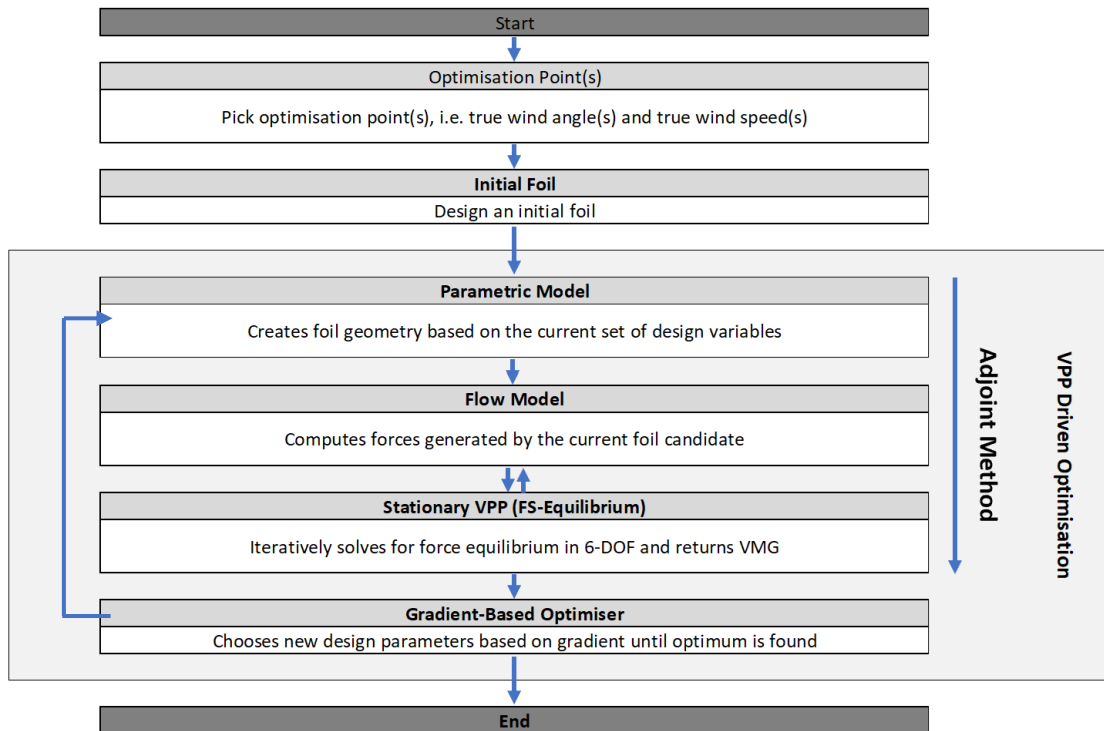

Figure 16. Adjoint VPP driven optimisation strategy.

8. AKNOWLEDGEMENTS

9. REFERENCES

America´s Cup (2020). Virtual Eye, (viewed 8-Dec-2022), https://ac36.americascup.com/en/advanced-dashboard.

Bingol, O. 2022. NURBS-Python Visualization, (viewed 5-Dec-2022), python.readthedocs.io/en/5.x/visualization.html.

Eggert, F (2018), Flight Dynamics and Stability of a Hydrofoiling International Moth with a Dynamic Velocity Prediction Program (DVPP), Masters of Science in Naval Architecture and Ocean Engineering thesis, Technische Universität Berlin.

Faltinsen, O. (2005). *Hydrodynamics of High-Speed Marine Vehicles*. Cambridge University Press, Cambridge, UK.

Gattini, S. (2020). PRADA ACWS - Day 1 Photo Gallery, (viewed 22-Jun-2021), https://www.lunarossachallenge.com/en/gallery/614_PRADA-ACWS-Day-1-Photogallery.

Hazen, G.S. (1980). A Model of Sail Aerodynamics for Diverse Rig Types, The New England Yacht Symposium.

Hansen H., Hochkirch K., Burns I., and Ferguson S. (2019). Maneuver Simulation and Optimization for AC50 Class, *Journal of Sailing Technology*, 4, 142-160.

Hochkirch, K. (2018). FS-Equilibrium User Manual.

Hoerner, S. F. (1965). *Fluid-Dynamic Drag*. Published by the Author.

Jayaraman, P. 2022. GitHub – TinyNURBS, (viewed 31-May-2022), https://github.com/pradeeppyro/tinynurbs.

Larsson, L., Eliasson, R. E., and Orych, M. (2014). *Principles of Yacht Design*. International Marine/McGraw Hill Education, 4th Edition, Camden, Maine.

Melis, F. M., Hansen H., Fischer, M. and Abdel-Maksoud, M. (2022). Velocity Prediction Program for a Hydrofoiling Lake Racer. *Journal of Sailing Technology*, 7, 255-275.

Molland, A. F. and Turnock, S. R. (2021). *Marine Rudders, Hydrofoils and Control Surfaces.* Butterworth Heinneman, 2nd Edition, Oxford, UK.

Molland, A. F., Turnock, S. R. and Hudson D. A. (2017). *Ship Resistance and Propulsion.* Cambridge University Press, 2nd Edition, Cambridge, United Kingdom.

Patterson, N. and Binns, J. (2022). Development of a Six Degree of Freedom Velocity Prediction Program for the foiling America's Cup Vessels. *Journal of Sailing Technology*, 7, 120-151.

Paulin A., Hansen H., Hochkirch K. and Fischer M. (2015). Performance Assessment and Optimization of a C-Class Catamaran Hydrofoil Configuration, 5th High Performance Yacht Design Conference Auckland, New Zealand.

Phillips, W. F. and Snyder, O. D. (2000). Modern Adaptation of Prandtl's Classic Lifting-Line Theory. *Journal of Aircraft,* 3, 662-670.

Piegl, L. and Tiller, W. (1997). *The NURBS Book.* Springer, 2nd Edition.

Prandtl, L. (1918). *Tragflügeltheorie.* Königliche Gesellschaft der Wissenschaften zu Göttingen, Göttingen, Germany.

Press, W. H., Flannery, B. P., Teukolsky, S. A. and Vetterling, W. T. (1988). *Numerical recipies in C.* Cambridge University Press, New York.

Reid, J. T. (2020). A General Approach to Lifting Line Theory, Applied to Wings with Sweep. All Graduate Theses and Dissertations. 7842.

Royal New Zealand Yacht Squadron, Circolo Della Vela Sicilia (2020). AC75 Class Rule v1.16.

Royal New Zealand Yacht Squadron, Royal Yacht Squadron (2023). AC75 Class Rule v2.9.

Specialist Committee of 23rd ITTC (2002). Recommended Procedures and Guidelines - Testing and Extrapolation Methods, Resistance Uncertainty Analysis, Example for Resistance Test. International Towing Tank Conference.

Whicker, L. F. and Fehlner, L. F. (1958). Free-Stream Characteristics of a Family of Low-Aspect Ratio, All Moveable Control Surfaces for Application to Ship Design.